Yuan *et al. Chem. Biol. Technol. Agric.* (2024) 11:18
https://doi.org/10.1186/s40538-024-00539-3

Chemical and Biological Technologies in Agriculture

RESEARCH

Open Access

# Structural characterization of a low-molecular weight linear *O*-acetyl-glucomannan in *Lilium lancifolium* from Tibet and its protected $H_2O_2$-induced oxidative stress in HUVEC cells

Lei Yuan[1,2,3,4], ZhengChang Zhong[1,4], Yu Liu[1,4], Hong Quan[1,5] and XiaoZhong Lan[1,2,3,4*]

**Abstract**

In recent years, the biological activity of plant polysaccharides has received increasing attention. Polysaccharides, as one of the main components of lilies, have pharmacological effects in regulating immunity, anti-tumor, antioxidant, antibacterial, and hypoglycemic effects. To systematically analyze the structural characteristics of the polysaccharide, the polysaccharide LP-1 was prepared from *Lilium lancifolium* bulbs by water extraction and ethanol precipitation, ion exchange chromatography and gel filtration chromatography. Structural characterizations show that the weight-average relative molecular weight of LP-1 is 5.3 kDa. LP-1 consists of mannose and glucose at a molar ratio of 1.4:1. Its primary structure is Glc*p*-α-D-(1 → {4)-β-D-Glc*p*-(1 → 4)-β-D-2-*O*-acetyl-Man*p*-(1 → [4)-β-D-Glc*p*-(1 → 4)-β-D-Glc*p*-(1 → 4)-β-D-Man*p*-(1 → 4)-β-D-Man*p*-(1 → 4)-β-D-Man*p*-(1 → 4)-β-D-Man*p*-(1]$_2$}$_2$ → 4)-α-D-Glc*p*. Acetylation occurs at the *O*-2 site of mannose. Acetyl substitution degree is 8.21%. The results of structure elucidation showed that LP-1 was a low-molecular weight linear *O*-acetylated glucomannan. The results of oxidative stress experiments indicate that LP-1 exerts antioxidant effects on HUVEC by activating the Nrf2/HO-1 signaling pathway, thereby improving endothelial cell damage induced by $H_2O_2$, and has the potential to be developed as an antioxidant drug.

**Keywords** *Lilium lancifolium*, Polysaccharide, Glucomannan, Structural characteristics, Oxidative stress

*Correspondence:
XiaoZhong Lan
lanxiaozhong@163.com
Full list of author information is available at the end of the article

**Graphical Abstract**

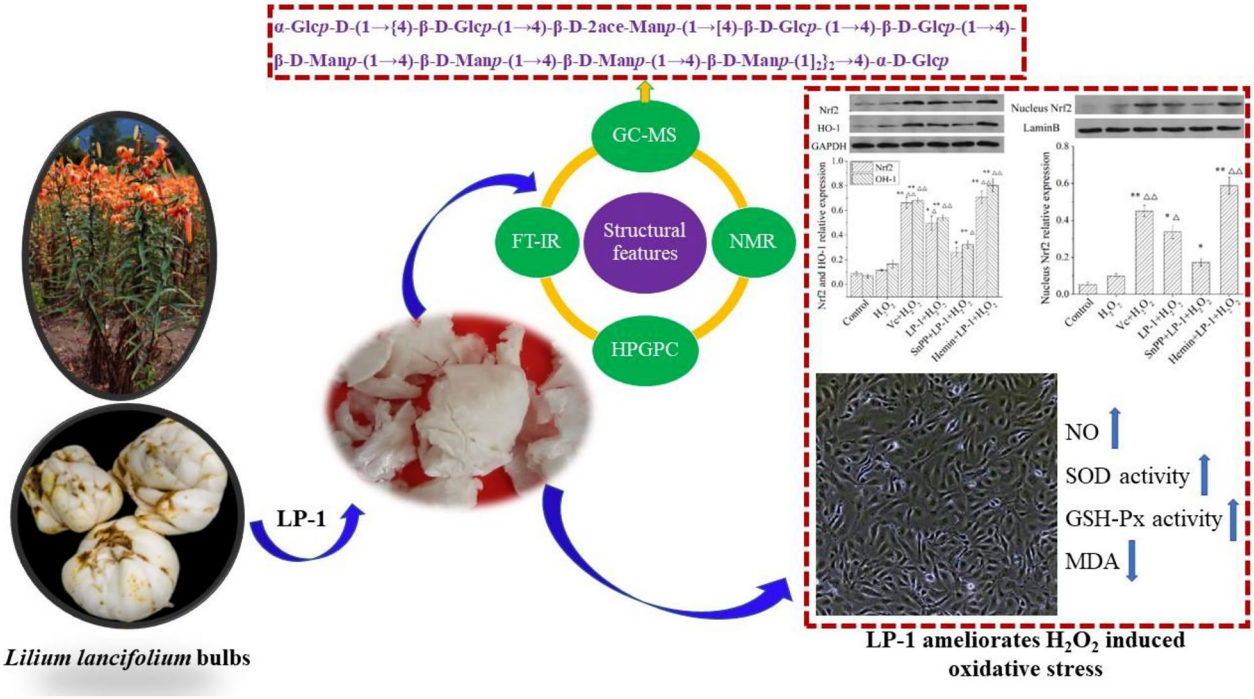


## Introduction

*Lilium* is widely cultivated for its edible bulb, which has been considered a food and traditional herb with high nutritional and medicinal value in East Asia for hundreds of years. Bulbs are not only rich in nutrients such as carbohydrates, amino acids, dietary fiber, and minerals, but also contain abundant physical and chemical substances such as phenols, flavonoids, polysaccharides, and alkaloids [1, 2]. Therefore, *Lilium* has been included in the first batch of medicinal and edible homologous plant lists approved by the Ministry of Public Health of China [3]. As a traditional Chinese medicine, *Lilium* was first identified in Shen Nong's Herbal Classic in the Eastern Han Dynasty of China. It is known to moisten the lung, relieve fever, calm nerves and treat continuous cough, hemoptysis, anxiety, insomnia and dreaminess [4]. Polysaccharides, as one of the main ingredients of *Lilium*, exert pharmacological effects on immune regulation, anti-tumor, anti-oxidation, bacteriostasis and blood sugar reduction [5–13]. Therefore, the content of polysaccharides in *Lilium* is an important indicator for evaluating the quality of this herb in the Chinese Pharmacopoeia.

Glucomannans (GMs), most of which have acetyl groups, widely exist in Orchidaceae, Liliaceae, Araceae, Dioscoreaceae and other plants. In GMs, one or multiple acetyl groups generally connect to the *O*-2, *O*-3 or *O*-6 sites of mannose and/or glucose residues [14]. Acetyl groups have important effects on the solubility, viscosity, three-dimensional structure and other physical properties of GMs; they can also modulate the biological properties of these molecules, such as their antioxidant, immune regulatory, anti-radiation and bacteriostatic activity [14–19].

*Lilium lancifolium* is one of the original plants of medicinal *Lilium* recorded in the Chinese Pharmacopoeia. Recent research on *L. lancifolium* mainly focuses on molecular weight of its polysaccharides, monosaccharide composition and immune regulatory and antioxidant activity [3, 5, 6]. However, there have been no reports on the fine structure analysis and antioxidant stress research of polysaccharides from *Lilium lancifolium*. In this study, a low-molecular weight linear *O*-acetylated glucomannan (LP-1) is isolated from *L. lancifolium* bulbs. The structural characteristics of LP-1 are analyzed by Fourier transform infrared spectroscopy (FT-IR), methylation analysis, gas chromatography-mass spectrum (GC–MS) and 1D and 2D nuclear magnetic resonance spectroscopy (NMR), and its protective effect on $H_2O_2$-induced oxidative stress in Human Umbilical Vein Endothelial Cells (HUVEC) was studied.

## Materials and methods

### Materials and reagents

Bulbs of *L. lancifolium* collected from the Tibetan Medicine Planting Base of Tibet Agricultural and Animal Husbandry University (N: 29.77, E: 94.74) in October 2019, and the impurities were removed and dried at normal temperature for later use.

3-[4,5-dimethylthiazol-2-yl]-2,5-diphenyltetrazolium bromide (MTT), Monosaccharide standards were obtained from Sigma-Aldrich (USA). DEAE Sepharose Fast Flow and Sephacryl S-200HR were obtained from GE Healthcare (Sweden). Dextran standards were obtained from Waters Co. (USA). Fetal bovine serum (FBS) was obtained from ExCell Bio (China). Trypsin–EDTA, penicillin and streptomycin were obtained from Procell (China). The Nuclear factor E2 related factor 2 (Nrf2) and Nuclear Loading Control (laminB) antibodies were obtained from Affinity (China). The Hemeoxygenase-1 (HO-1) antibodies were obtained from Wuhan Sanying (China). Other reagents and chemicals were of analytical grade.

### Preparation of the *L. lancifolium* polysaccharide LP-1

Exactly 250 g of *L. lancifolium* bulbs was leached at 90 ℃ for 2 h according to a solid–liquid ratio 1:12 and extracted three times. The leach liquor was combined and concentrated to 1/10 of the original volume. Four volumes of 95% ethanol were added to the liquor, and the mixture was allowed to precipitate for 24 h. The precipitation was collected after centrifugation at 4000 rpm for 10 min. The precipitate was dissolved in distilled water and freeze-dried to obtain crude polysaccharide CLP, weighed, and yield calculated.

CLP was subjected to ion exchange chromatography on DEAE Sepharose Fast Flow (3.5 × 47.0 cm), eluted with distilled water to obtain the neutral polysaccharide CLP-1. Then, CLP-1 was purified using Sephacryl S-200HR (2.5 cm × 100.0 cm) and eluted with 0.9% sodium chloride. Subsequently, one homogeneous neutral polysaccharide component LP-1 was obtained.

### Structural analysis of LP-1

#### *General analysis of LP-1*

The proportions of sugar and protein in LP-1 were determined using the phenol–sulfuric acid and Bradford methods.

#### *Molecular weight determination*

Glucans with different molecular weights (*MW* 1,152, 11,600, 23,800, 48,600, 80,900, 148,000, 273,000, 410,000 Da) were precisely weighed. Distilled water prepared as 5 mg/mL standard solution was added, and the clarified liquid filtered by a 0.22-μm microporous membrane was taken. Standard curves of glucans with different molecular weights were determined by high-performance gel permeation chromatography (HPGPC). The purified LP-1 solution was prepared according to the same steps, and the concentration was 5 mg/mL polysaccharide solution. The molecular weight and homogeneity of the polysaccharide sample were determined by HPGPC method. HPGPC: LC-10A (Shimadzu Co., Ltd., Japan); chromatographic column: BRT105-104–102 tandem gel column (8 × 300 mm); mobile phase: 0.05 mol/L NaCl solution; flow rate: 0.6 mL/min, column temperature: 40 °C; injection volume: 20 μL; detector: differential detector RI-10A.

#### *Monosaccharide composition*

A Dionex Ion Chromatography ICS 5000 system (Thermo Fisher Scientific Inc., USA) and a CarboPac PA20 analytical column (150 × 3 mm) (Thermo Fisher Scientific Inc., USA) were used to analyze the monosaccharide composition of the LP-1. LP-1 (4 mg) was hydrolyzed for 4 h with 1 mL of 2 M trifluoroacetic acid at 120 ℃. Excess trifluoroacetic acid was removed through reduction vaporization at 55 ℃. The residues were dissolved in 4 mL of methanol and evaporated to dryness; this step was repeated four times. The residue was re-dissolved in 10 mL of distilled water. Solvent A was water, solvent B was 250 mM NaOH and C was 50 mM NaOH and 500 mM $CH_3COONa$. Flow rate: 0.3 mL/min; injection sample volume: 5 μL; column temperature: 30 °C; detector: electrochemical detector.

#### *FT-IR spectroscopy*

KBr and LP-1 were pressed into disks. A Fourier transform infrared spectrophotometer (is50, Thermo Fisher Scientific Inc., USA) was used to collect the FT-IR spectra of the samples over the wavenumber range of 4000–400 $cm^{-1}$.

#### *Methylation analysis*

Methylation and GC–MS analyses were conducted according to a previously reported method [20]. LP-1 (3.0 mg) was dissolved in anhydrous DMSO (1.0 mL), and 20–30 mg NaOH and 1 mL $CH_3I$ were added for 60 min. Methylation was terminated by addition of 2 mL of ultrapure water. Methylated LP-1 was hydrolyzed with 2 M $CF_3COOH$ (1 mL) at 120 °C for 90 min and then evaporated to dryness. The hydrolysate was then reduced with 60 mg NaBH4 for 8 h and acetylated with 1 mL $Ac_2O$-pyridine (1:1, v/v) at 100 °C for 1 h. Analytical instruments: GCMS-QP2010 plus (Shimadzu Co., Ltd., Japan) equipped with a Rxi-5Sil MS column (30 m × 0.25 mm × 0.25 μm). Temperature programmed: initial temperature of 120 °C, which was raised to 250 °C/

min at 3 °C/min and maintained for 5 min; ion source temperature 250 °C; injector temperature of 250 °C; and flow rate of He at 1 mL/min. Characterization of the partially methylated alditol acetates (PMAAs) peaks was achieved by determining their retention times and cleavage modes and comparison with the mass spectrometric data in the literature [21].

#### *NMR spectroscopy*

Exactly 50 mg of LP-1 was dissolved in 0.5 mL of $D_2O$ for freeze-drying. The above process was repeated to exchange active hydrogen in the sample completely. Then, the sample was dissolved in 0.5 mL of $D_2O$ and NMR (1D and 2D) spectra, inclusive of $^1$H(500 MHz), $^{13}$C(126 MHz), $^1$H-$^1$H COSY, HSQC, HMBC, and NOESY were recorded at 25 °C with a Bruker AV500M NMR spectrometer (Bruker, Germany). MestReNova software was used to process and analyze data.

The DA of LP-1 could be determined from the $^1$H NMR data by the following formula [22]:

$$\mathrm{DA} = \left[\frac{\left(I_{\mathrm{CH_3}} \times 100\%\right)/3}{I_{\sum \mathrm{H1}}}\right],$$

where $I_{CH3}$ refers to the integral of the hydrogen atom in $-COCH_3$ group and $I\sum_{H1}$ the total integral of the anomeric proton in glucose and mannose.

### Effect of LP-1 on $H_2O_2$ induced oxidative stress in HUVEC cells

#### *Cell culture*

HUVEC cells (GuangZhou Jennio Biotech Co., Ltd., China) were maintained in ECM (ScienCell Research Laboratories, Inc., USA) supplemented with 10% FBS, 1% penicillin and streptomycin, at 37 °C with 5% $CO_2$. All treatments were performed when the cells density reached about 80%.

#### *Cell viability determination*

Control group, Model group (0.2 mM $H_2O_2$), Vc group (0.2 mM $H_2O_2$ + 100 μg/mL Vc), and LP-1 group (0.2 mM $H_2O_2$ + 100, 400, 800 μg/mL LP-1) were established for cell viability studies. HUVEC cells ($5.0 \times 10^3$ cells/mL) were inoculated into a 96-well cell culture plate. After culture overnight at 37 °C, Vc and LP-1 of different concentrations were added to the Vc group and LP-1 group. The control group and model group were given equal volume complete culture medium, and co-cultured with cells under conventional conditions for 20 h. Discard the medium, and serum-free medium (100 μL) with $H_2O_2$ concentration of 0.2 mM to each well for 24 h and then added with 10 μL of MTT. After incubation at 37 °C for 4 h, the culture was terminated. The absorbance (A) of the solutions in each well at a wavelength of 568 nm was detected. Inhibition rate (%) = [(Control group − Experimental group)/(Control group-Blank group)] × 100%.

#### *Determination of NO*

The concentration of nitric oxide (NO) in cell supernatant of each group was detected by Griess method (Nanjing Jiancheng, China). Cultivate HUVEC cells according to the method in 2.4.2 and collect the supernatant. Take a 96-well plate and add 50 μL standard and sample, then add 50 μL Griess Reagent I and Griess Reagent II solutions respectively, incubate at room temperature for 10 min, and measure the absorbance of each well at a wavelength of 550 nm using an enzyme-linked immunosorbent assay (ELISA) reader (Flexstation3, Molecular Devices, USA). Calculate the concentration of NO in the sample based on the standard curve.

#### *Determination of SOD, GSH-Px and MDA*

Cultivate HUVEC cells according to the method in 2.4.2 and cells in the culture plate were washed with PBS. Then cells were detached from the plate by adding 200 μL of trypsin solution per well, resuspended in complete medium and centrifuged at 4000 rpm for 15 min. Afterward, the supernatant was discarded, and the process was repeated once. Then, the 1.0 mL lysate was added to the cell, and the lysate cells were centrifuged for 5 min (12,000 rpm), and the supernatant was taken out. The levels of SOD, GSH-Px and MDA in the cell homogenate were determined according to the instructions of the corresponding kits (Nanjing Jiancheng Bioengineering Institute, China).

#### *Western blot*

After each group of cells were treated, they were washed thrice with pre-cooled PBS. Cell lysate containing benzoyl sulflulfluoride and protease inhibitors were added for lysis. The lysate was collected and then centrifuged at 12,000 rpm for 20 min at 4 °C. The cell liquid was retained, and the BCA method was used to determine protein concentration. After adjusting to a uniform mass concentration, it was cooked at 100 °C for 10 min to denature the protein. Denaturing polyacrylamide gel electrophoresis was carried out, and the membrane was transferred, blocked, and added with corresponding primary antibody for subsequent incubation overnight at 4 °C. The mixture was washed for five times with TBST to incubate the HRP-labeled secondary antibody. ECL kit was used for development, and the imaging system development and IPP software were used to analyze the band gray value.

### Statistical analysis

IBM SPSS 19.0 statistical software was used for statistical analysis. The experiment was repeated three times, and relevant data were expressed as the mean ± standard deviation (mean ± SD). The significance of differences between the groups was analyzed with completely random one-way ANOVA, and Origin 8.1 software was used for plotting. A $p$ value of less than 0.05 was considered statistically significant.

## Results and discussion

### Analysis of physical and chemical properties of LP-1

The extraction temperature was 90 °C, and the extraction time was 2 h. Under the optimal technological conditions, the yield of CLP was 11.72% (calculated by the quality of dry sample). LP-1 was obtained by ion exchange chromatography and gel filtration chromatography. The total sugar and protein contents of LP-1 were 93.34% and 1.59%, respectively. The HPGPC results of polysaccharides in *L. lancifolium* are shown in Fig. 1a. A single symmetric peak could be observed in the figure, thereby indicating that LP-1 has good uniformity. The regression equation log $MW = -0.1981x + 12.519$ ($R^2 = 0.9941$) was obtained by taking the retention time as the abscissa and the log $MW$ as the ordinate. The retention time of LP-1 was 44.406 min. Thus, according to the regression equation, the molecular weight of LP-1 is 5.3 kDa.

The monosaccharide composition of LP-1 is shown in Fig. 1b. LP-1 is composed of mannose and glucose at a molar ratio is 1.4:1.

The FT-IR spectrum of LP-1 is shown in Fig. 1c. The broad and strong absorption peak at 3,400 $cm^{-1}$ is attributed to the stretching vibrations of O–H, and the peak at 2930 $cm^{-1}$ is attributed to the stretching vibrations of C–H [23]. C=O covalent vibrations, C–H bending vibrations and C–O vibrations of the acetyl group are indicated by peaks at 1731, 1377 and 1249 $cm^{-1}$ [24, 25]. These results indicate that LP-1 is a type of acetylated polysaccharide. The characteristic peaks of β-glucose and β-mannose are mainly observed at 890 and 807 $cm^{-1}$, respectively [26, 27].

The methylation products of LP-1 were hydrolyzed and acetylated for GC–MS analysis, and the results are shown in Fig. 1d and Table 1. LP-1 is mainly composed of Glc*p*-1 →, → 4-Man*p*-1 → and → 4-Glc*p*-1 → at a molar ratio of 1.0:8.8:5.3.

### NMR spectroscopy

The $^1$H NMR spectrum of LP-1[1] (500 MHz, $D_2O$) is shown in the Fig. 2a. Five anomeric proton signals could be observed in the spectrum, and the chemical shifts of these signals are 5.33, 5.32, 4.85, 4.67 and 4.41 ppm. The sugar residues were numbered as A–E according to the decreasing chemical shift of anomeric proton. The $^{13}$C

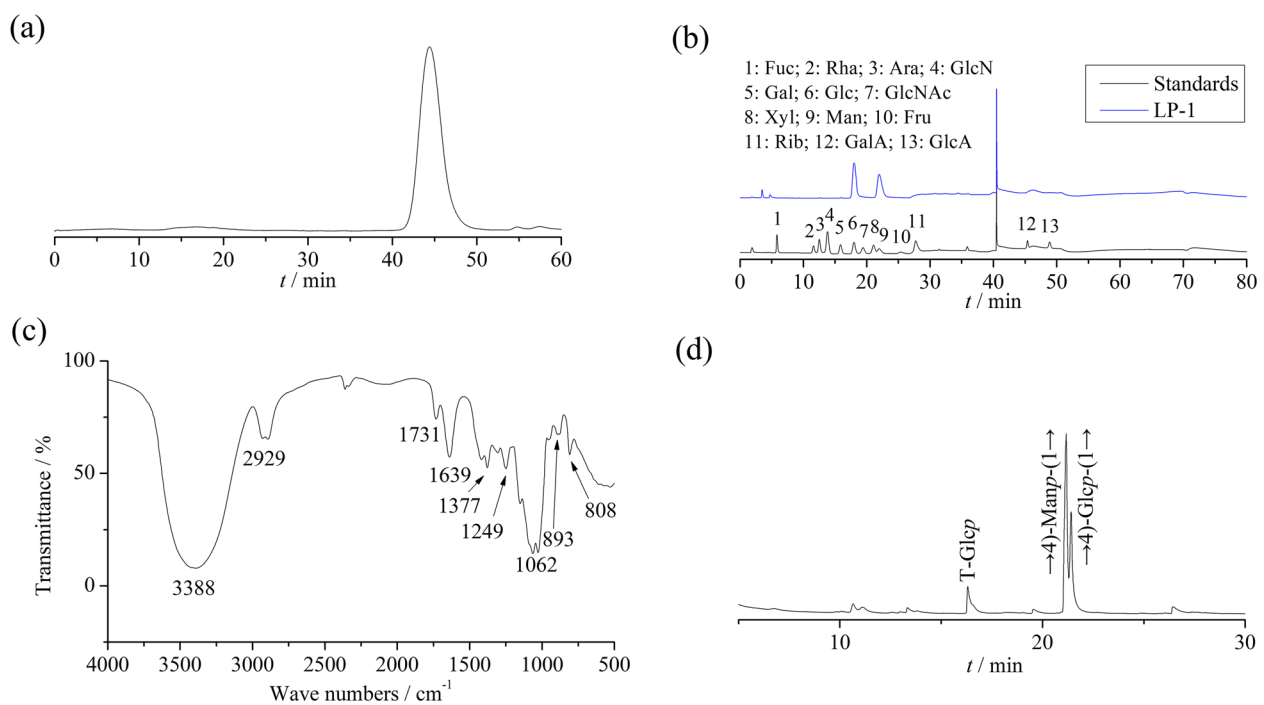


**Fig. 1** Physical and chemical properties of LP-1. **a** HPGPC profiles of LP-1; **b** monosaccharide composition of LP-1 analyzed by HPAEC-PAD chromatograms; **c** FT-IR spectrum of LP-1; **d** the total ion chromatogram from methylation analysis of LP-1

**Table 1** Methylation analysis of LP-1

| Methylated sugars | Linkages | Molar ratio | Major mass fragments (*m/z*) |
|---|---|---|---|
| 2,3,4,6-$Me_4$-Glc*p* | Glc*p*-(1 → | 1.0 | 43,71,87,101,117,129,145,161,205 |
| 2,3,6-Me3-Man*p* | → 4)-Man*p*-(1 → | 8.8 | 43,87,99,101,113,117,129,131,161,173,233 |
| 2,3,6-Me3-Glc*p* | → 4)-Glc*p*-(1 → | 5.3 | 43,87,99,101,113,117,129,131,161,173,233 |

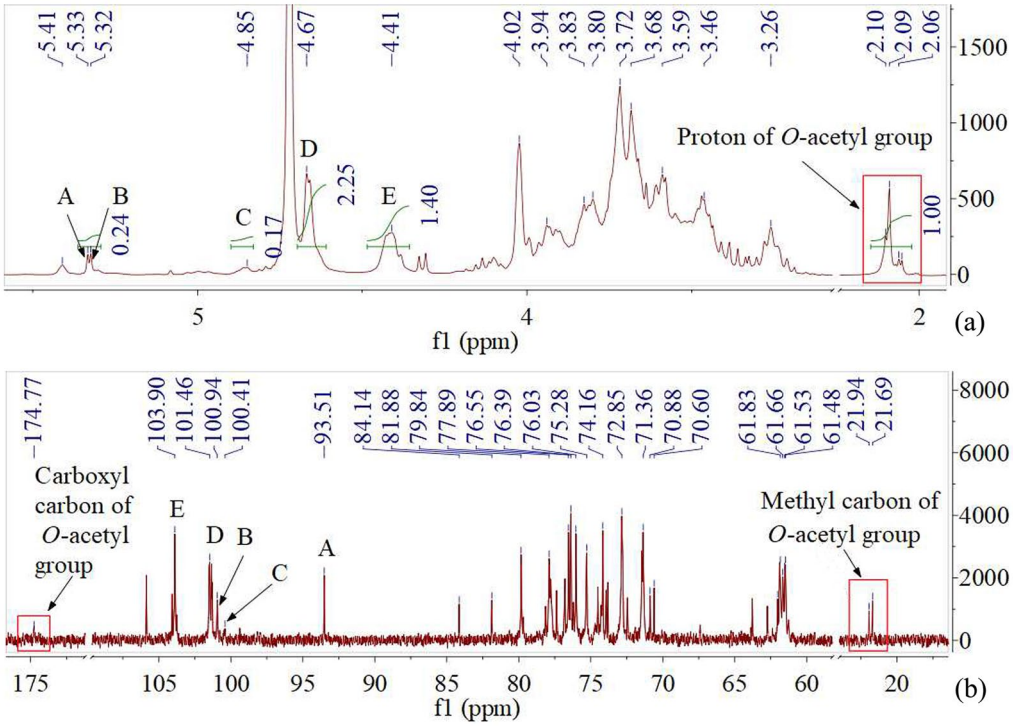


**Fig. 2** NMR spectra of LP-1. $^{1}$H- (**a**) and $^{13}$C- (**b**) NMR spectra

NMR spectrum (126 MHz, $D_2O$) is shown in Fig. 2b. The chemical shifts of the main anomeric carbons of LP-1 are observed at 103.90, 101.46, 100.94, 100.41 and 93.51 ppm. The signals near 2.10 ppm in the $^{1}$H NMR spectrum and the signals of 21.69 and 174.77 ppm in the $^{13}$C NMR spectrum are characteristic signals of the *O*-acetyl group. Substitution of *O*-acetyl groups leads to the chemical shifting of non-anomeric hydrogens on the sugar ring to a lower field (4.3–5.9 ppm). The $^{1}$H NMR spectrum of LP-1 also shows a characteristic absorption signal between 5.40 and 5.50 ppm (~5.41 ppm), which could be attributed to →4)-β-Man*p*-(1→ residues with *O*-2 substituted by acetyl groups [28–32].

The anomeric proton of LP-1 and the integral of the hydrogen atom in the $-COCH_3$ group are shown in Fig. 2a. The degree of acetylation substitution of LP-1 DA = [(1 × 100%)/3]/(0.24 + 0.17 + 2.25 + 1.40) ≈ 8.21%.

The HSQC spectrum (Fig. 3a) revealed five coupling peaks in the heterocephalic region; these peaks are located at δ 5.33/93.51, δ 5.31/100.41, δ 4.85/101.46, δ 4.66/100.94 and δ 4.40/103.90 and respectively correspond to H-1/C-1 of →4)-α-D-Glc*p* (A), Glc*p*-α-D-(1→(B), →4)-2-*O*-acetyl-β-D-Man*p*-(1→(C), →4)-β-D-Man*p*-(1→(D) and →4)-β-D-Glc*p*-(1→(E). A δ 5.41/72.52 coupling peak, which is attributed to H-2/C-2 of C, is also detected in the HSQC spectrum. The chemical shifts of C and H in LP-1 were determined by analyzing the HSQC and H–H COSY (Fig. 3b) data based on the anomeric carbons and proton , while referring to the methylation results of the same sugar residues and the relevant literature. [29, 33–42]. The attribution results are shown in Table 2.

The combined results of the HMBC (Fig. 3c) and NOESY (Fig. 3d) spectra were used to analyze the connection mode of the polysaccharide. The anomeric hydrogen of →4)-α-D-Manp-(1→(D) and its C-4 show a correlated signal peak (δ 4.67/77.93), and the anomeric carbon of D and its H-4 show a correlated signal

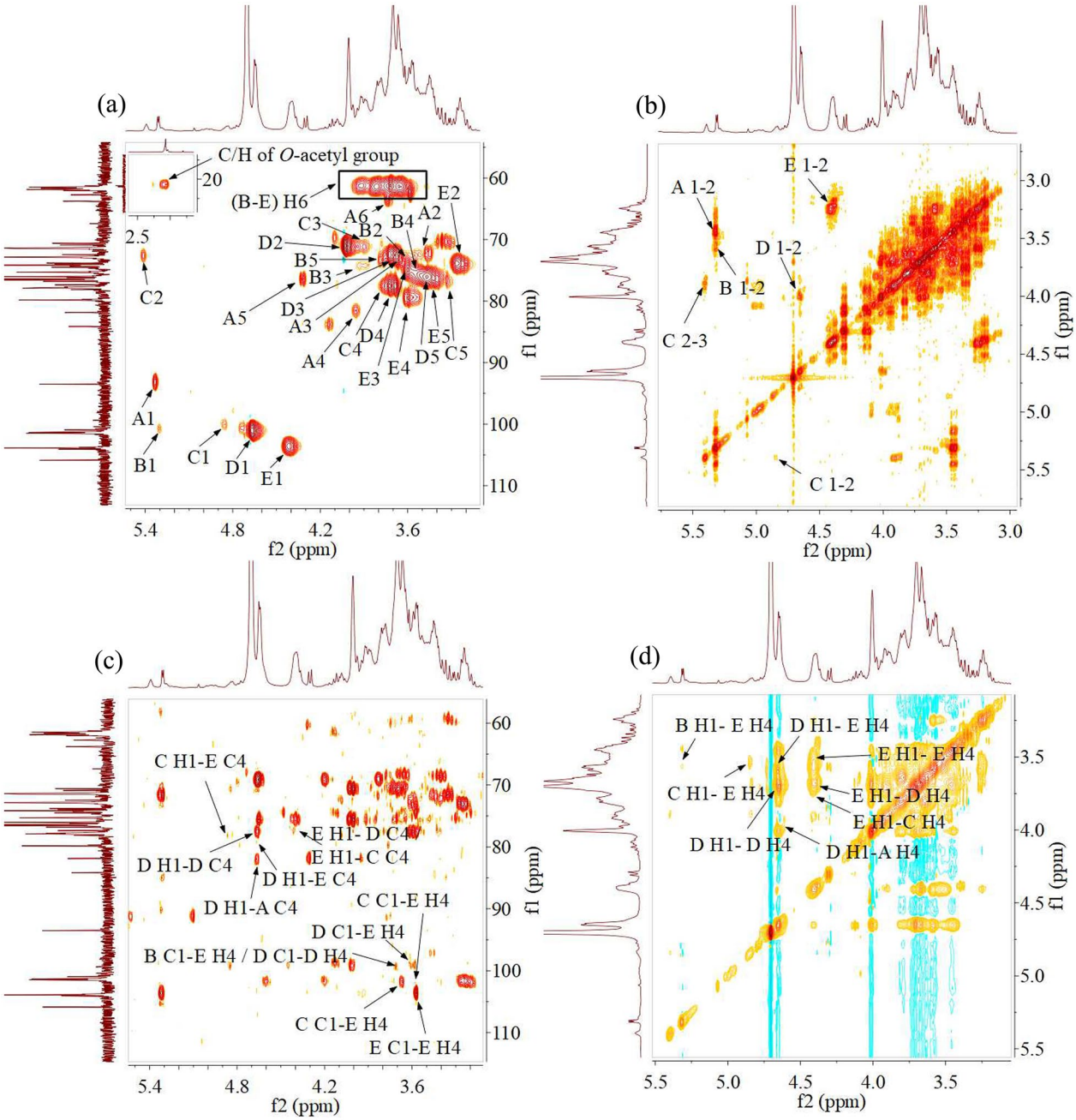


**Fig. 3** NMR spectra of LP-1. $^{1}$H-$^{13}$C HSQC (**a**), $^{1}$H-$^{1}$H COSY (**b**), HMBC (**c**) and $^{1}$H-$^{1}$H NOESY (**d**) spectra

(δ 100.94/3.71). The NOESY spectrum reveals a correlated signal between the anomeric hydrogen of D and its H-4 (δ 4.67/3.71e), which indicates a connection mode of →4)-α-D-Manp-(1→4)-α-D-Manp-(1→. Other connection modes were analyzed according to the above method. The HMBC and NOESY correlation signal for the linkage sequence are shown in Table 3. The structure of LP-1 was finally obtained as follows: Glcp-α-D-(1→{4)-β-D-Glcp-(1→4)-β-D-2-*O*-acetyl-Manp-(1→[4)-β-D-Glcp-(1→4)-β-D-Glcp-(1→4)-β-D-Manp-(1→4)-β-D-Manp-(1→4)-β-D-Manp-(1→4)-β-D-Manp-(1]$_2$}$_2$→4)-α-D-Glcp.

In recent years, there are many reports on the structural identification of *Lilium* polysaccharides, mainly concentrated on *L. brownii* F. E. Br. ex Miellez, *L. davidii*

**Table 2** $^{1}H$ and $^{13}C$ NMR spectrum assignments for LP-1

| Glycosyl residues | H1<br>C1 | H2<br>C2 | H3<br>C3 | H4<br>C4 | H5<br>C5 | H6a<br>C6 | H6b |
|---|---|---|---|---|---|---|---|
| →4)-α-D-Glcp<br>(A) | 5.33<br>93.51 | 3.45<br>72.44 | 3.67<br>72.57 | 3.95<br>81.91 | 4.32<br>76.82 | 3.73<br>63.73 | |
| Glcp-α-D-(1→<br>(B) | 5.32<br>100.41 | 3.56<br>72.88 | 3.89<br>74.67 | 3.57<br>75.11 | 3.76<br>73.34 | 3.78<br>61.95 | 3.66 |
| →4)-2-*O*-acetyl-β-D-Man*p*-(1→<br>(C) | 4.85<br>101.46 | 5.41<br>72.60 | 3.91<br>71.30 | 3.78<br>77.60 | 3.37<br>76.10 | 3.76<br>61.82 | 3.63 |
| →4)-β-D-Manp-(1→<br>(D) | 4.67<br>100.94 | 4.02<br>71.38 | 3.72<br>72.43 | 3.71<br>77.93 | 3.45<br>76.07 | 3.81<br>61.84 | 3.65 |
| →4)-β-D-Glcp-(1→<br>(E) | 4.41<br>103.90 | 3.24<br>74.17 | 3.57<br>74.63 | 3.58<br>79.46 | 3.41<br>76.69 | 3.89<br>61.67 | 3.73 |
| *O*-acetyl group | 174.77/21.69–21.94/2.06–2.10 | | | | | | |

**Table 3** HMBC and NOESY spectrum assignments for LP-1

| Connection mode | B→E | E→C | C→E | E→E | E→D | D→D | D→E | D→A |
|---|---|---|---|---|---|---|---|---|
| $H_1$<br>$C_n$ | – | 4.41<br>77.60 | 4.85<br>79.46 | – | 4.41<br>77.93 | 4.67<br>77.93 | 4.67<br>79.46 | 4.67<br>81.91 |
| $C_1$<br>$H_n$ | 100.41<br>3.58 | – | 101.46<br>3.58 | 103.90<br>3.58 | – | 100.94<br>3.71 | 100.94<br>3.58 | 100.94<br>3.95 |
| $H_1$<br>$H_n$ | 5.33<br>3.58 | 4.41<br>3.78 | 4.85<br>3.58 | 4.41<br>3.58 | 4.41<br>3.71 | 4.67<br>3.71 | 4.67<br>3.58 | 4.67<br>3.95 |

– Not detected

var. unicolor Cotton, *L. lancifolium* Thunb, etc., whose molecular weight distribution is wide, ranging from $4.79\times10^3$ to $8.52\times10^6$ Da, mainly composed of glucose, arabinose, rhamnose, xylose and galactose. Only Pan et al. reported an acetylated modified Lilium polysaccharide [43]. The structural characteristics of acetylated modified Lilium polysaccharides were analyzed in detail for the first time in this paper. This study laid a foundation for the structure–activity relationship analysis of LP-1.

## Effect of LP-1 on oxidative stress induced by hydrogen peroxide in HUVEC cells

### *LP-1 increases the activity of HUVEC cells induced by $H_2O_2$*

Compared with the control group, the cell viability of HUVEC induced by 0.2 mM $H_2O_2$ alone decreased significantly, while after pretreatment with LP-1 of different concentrations (100, 400, 800 μg/mL), the cell viability of HUVEC cells increased to a significant level ($p<0.05$) (Fig. 4a).

### *LP-1 attenuates $H_2O_2$-induced HUVEC cell damage*

The production or impaired bioavailability of NO is a common sign of endothelial dysfunction, and the production of nitrite (a stable metabolite of NO) is an indicator of NO production [44, 45]. Consistent with the loss of cell viability, $H_2O_2$ can reduce the formation of NO in HUVEC cells (Fig. 4b). However, the addition of LP-1 can inhibit the reduction of NO production induced by $H_2O_2$. Therefore, LP-1 can inhibit $H_2O_2$-mediated endothelial dysfunction in HUVEC cells.

MDA is a toxic substance produced by ROS acting on the cell membrane to produce chain reaction, causing lipid peroxidation. Its excessive accumulation will damage the cell membrane structure, leading to the overflow of cytoplasm and damaging the cell function [46]. Therefore, the oxidative damage of cells can be detected by the content of MDA [47]. As shown in Fig. 4c, compared with the control group, the MDA level in the model group increased significantly ($p<0.05$). In the experimental group, after the cells were treated with 100–800 μg/mL LP-1, the MDA level decreased compared with the model group, and the 800 μg/mL LP-1 group reached the extremely significant level, indicating that LP-1 can alleviate the damage caused by ROS to cells to a certain extent, and its protective effect gradually increased with the increase of concentration.

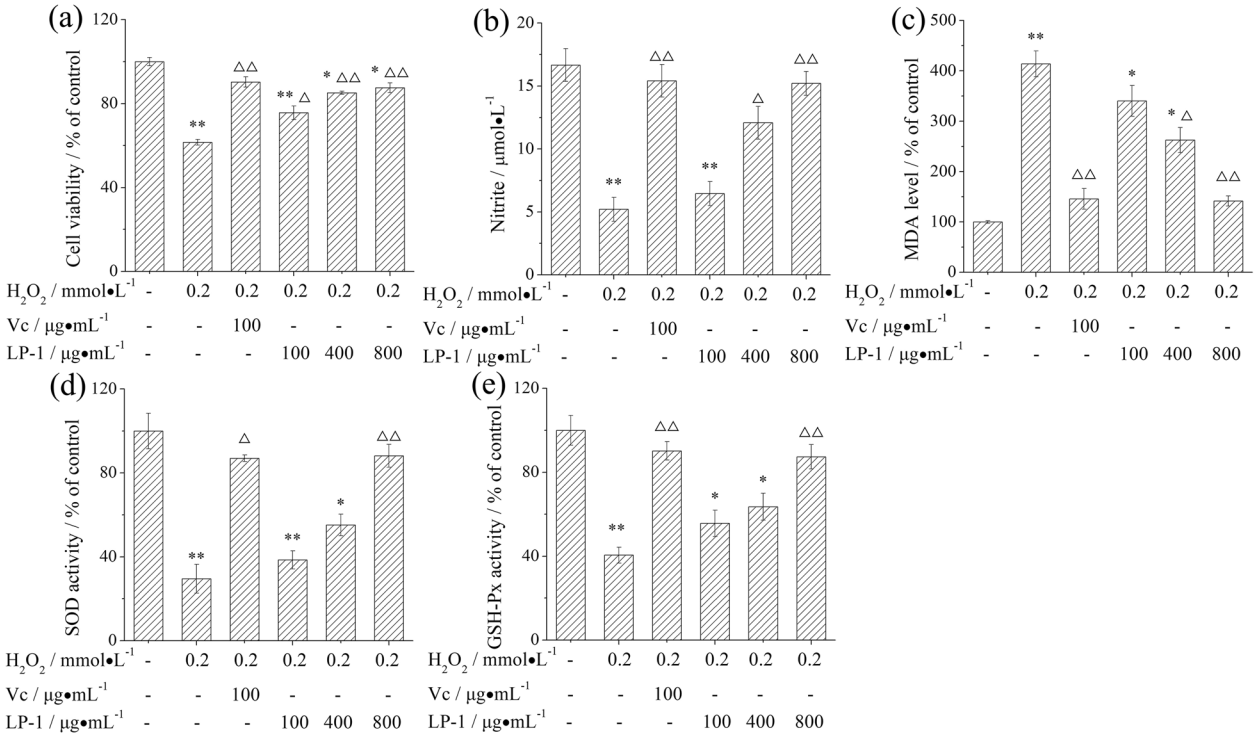


**Fig. 4** LP-1 ameliorates $H_2O_2$-induced oxidative stress. **a** Effect of LP-1 on cell viability in $H_2O_2$-treated HUVEC cells. **b** Effect of LP-1 on NO levels in $H_2O_2$-treated HUVEC cells. **c** Effect of LP-1 on MDA levels $H_2O_2$-treated HUVEC cells. **d** Effect of LBP on SOD activity in $H_2O_2$-treated HUVEC cells. **e** Effect of LBP on GSH-Px activity in $H_2O_2$-treated HUVEC cells. Data are presented as the mean ± SEM ($n = 3$). Compared with control group, *$p < 0.05$, **$p < 0.01$; Compared with model group, △$p < 0.05$, △$p < 0.01$

ROS is composed of hydrogen peroxide, superoxide anion, hydroxyl radical, singlet oxygen, etc. Inflammatory reaction, cold and heat stress, aging, ultraviolet radiation, and other internal and external factors will lead to the accumulation of ROS in cells. The elimination of ROS is an important way to protect organisms from oxidative stress damage, which is mainly achieved by antioxidant enzymes in the human body. SOD, CAT and GSH-Px belong to common antioxidant enzymes, which participate in the formation of biological defense system against oxidative damage and reduce the damage of ROS to cells [48–51]. The experiment preliminarily evaluated the antioxidant capacity of LP-1 by detecting the changes of SOD (Fig. 4d) and GSH-Px (Fig. 4e) activities in HUVEC cells. After $H_2O_2$ modeling, the activities of both enzymes were significantly reduced compared with control group ($p < 0.01$), and $H_2O_2$ significantly inhibited the activities of cell antioxidant enzymes. Compared with the model group, the activity levels of both enzymes in LP-1-treated cells were enhanced in a concentration-dependent manner. In the 800 μg/mL LP-1 group, SOD and GSH-Px activity increased significantly compared with the model group ($p < 0.01$). The above results showed that LP-1 could enhance the activity of SOD and GSH-Px in HUVEC cells under oxidative stress, and the effect was positively correlated with its concentration.

### *LP-1 inhibits oxidative stress by activating Nrf2/HO-1 signaling pathway*

Nrf2 is a key regulator to maintain redox homeostasis and cell antioxidant defense [52, 53]. It can regulate the expression of a variety of antioxidants and phase II detoxification enzymes through antioxidant response elements (ARE), HO-1, quinone oxidoreductase (NQO1), and SOD [54]. HO-1 can be used as an antioxidant enzyme to catalyze the degradation of heme to produce iron, carbon monoxide (CO), biliverdin and other metabolites, thus playing an anti-inflammatory, antioxidant, anti-apoptotic and other roles. A large number of studies have confirmed that the up-regulation of HO-1 expression helps cells resist external stimuli and respond to oxidative stress damage [55–57]. To explore the potential mechanism of LP-1 protecting endothelial cells from injury, we treated HUVEC cells induced by $H_2O_2$ with HO-1 inhibitor and activator, and measured the levels of NO, MDA, SOD, GSH-Px (Fig. 5a–d). The results showed that the protective effect of LP-1 on $H_2O_2$-induced endothelial cell injury was eliminated by HO-1 inhibitor, indicating

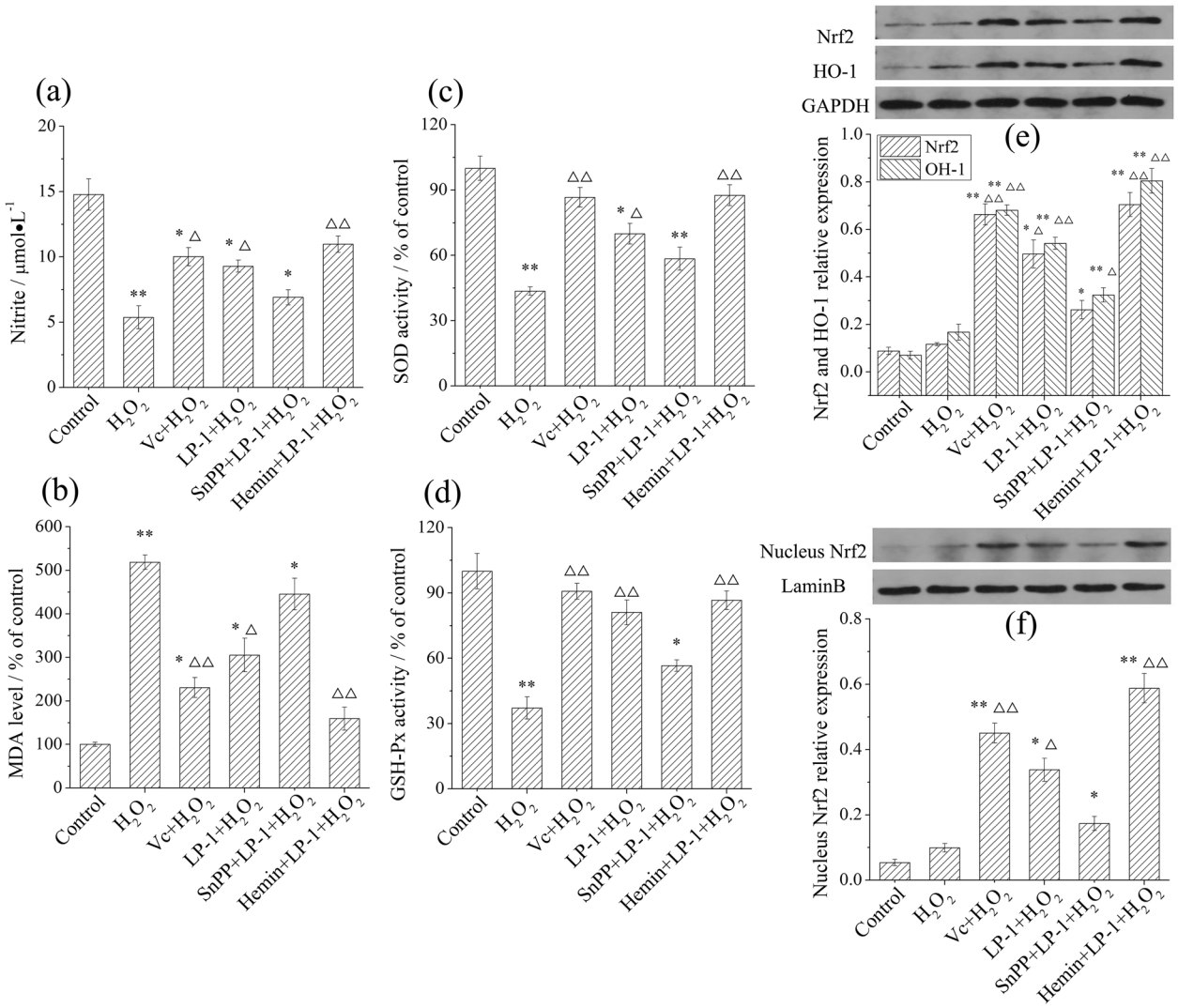


**Fig. 5** LP-1 alleviates $H_2O_2$-induced HUVEC cell damage via the Nrf2/HO-1 pathway. **a**–**d** Effects of HO-1 inhibitor and activator treatment on NO, MDA, SOD, GSH-Px levels in $H_2O_2$-induced HUVEC cells. **e** The relative protein expression levels of Nrf2 and HO-1 were determined via western blotting. **f** Western blot analysis was performed to detect the protein expression levels of nuclear Nrf2. Compared with control group, $^{*}p < 0.05$, $^{**}p < 0.01$; compared with model group, $\Delta p < 0.05$, $\Delta p < 0.01$

that the protective effect of LP-1 in oxidative stress depended on the activity of HO-1, and HO-1 activator could enhance the protective effect of LP-1. Furthermore, we detected the expression of Nrf2 and HO-1 proteins through the WB experiment (Fig. 5e, f). The results showed that LP-1 could up-regulate the expression of Nrf2 and nuclear translocation, and activate Nrf2/HO-1 signaling pathway. After the use of the HO-1 specific inhibitor SnPP, the effect of LP-1 on the up-regulation of Nrf2 and HO-1 protein expression in cells was lost, while the HO-1 activator could enhance the expression of Nrf2 and HO-1 protein, indicating that LP-1 could activate Nrf2/HO-1 signaling pathway to play a protective role and alleviate $H_2O_2$-induced endothelial cell damage.

The antioxidant activity of *Lilium* polysaccharides is one of their main biological activities. The results of this study indicate that LP-1 has an inhibitory effect on oxidative stress, which is consistent with the antioxidant effects of various *Lilium* polysaccharides reported by Guo et al. [43].

## Conclusions

In this paper, a low-molecular weight linear *O*-acetylated glucomannan (LP-1) was separated from bulbs of *L. lancifolium*. The structural characteristics of LP-1 were

analyzed by high-performance liquid chromatography, IR spectroscopy, methylation analysis, NMR spectroscopy and other technologies. The repeating structural units of the polysaccharide were also predicted. The results of oxidative stress experiments indicate that LP-1 exerts antioxidant effects on HUVEC by activating the Nrf2/HO-1 signaling pathway, thereby improving endothelial cell damage induced by $H_2O_2$, and has the potential to be developed as an antioxidant drug.

**Acknowledgements**
Not applicable.

**Author contributions**
LY wrote the main manuscript. XZL revised the manuscript and funding acquisition. ZCZ, YL, HQ reviewed and edited the manuscript. All authors reviewed the manuscript.

**Funding**
This research was funded by Tibet Autonomous Region Major Special Science and Technology, grant number: XZ202101ZD0023G; the Forth National Survey of Traditional Chinese Medicine Resources, Chinese or Tibet Medicinal Resources Investigation in Tibet Autonomous Region, grant number: State Administration of Chinese Traditional Medicine 20200501-542301; the Tibet Agriculture and Animal Husbandry University Project for Discipline Construction, Grant Number: 533323001.

**Availability of data and materials**
Not applicable.

## Declarations

**Ethics approval and consent to participate**
Not applicable.

**Consent for publication**
Not applicable.

**Competing interests**
The authors declare that they have no competing interests.

**Author details**
[1]The Provincial and Ministerial Co-Founded Collaborative Innovation Center for R & D in Tibet Characteristic Agricultural and Animal Husbandry Resources, Tibet Agriculture and Animal Husbandry University, Nyingchi 860000, Tibet, China. [2]The Center for Xizang Chinese (Tibetan) Medicine Resource, Tibet Agriculture and Animal Husbandry University, Nyingchi 860000, Tibet, China. [3]Joint Laboratory for Tibetan Materia Medica Resources Scientific Protection and Utilization Research of Tibetan Medical Research Center of Tibet, Nyingchi 860000, Tibet, China. [4]Natural Products Research Center, Tibet Agriculture and Animal Husbandry University, Nyingchi 860000, Tibet, China. [5]Research Institute of Plateau Ecology, Tibet Agriculture and Animal Husbandry University, Nyingchi 860000, Tibet, China.

Received: 21 November 2023 Accepted: 12 January 2024
Published online: 25 January 2024

**References**

1. Chen L, Yang YY, Zhou RR, Fang LZ, Zhao D, Cai P, et al. The extraction of phenolic acids and polysaccharides from lilium lancifolium thunb. Using a deep eutectic solvent. Anal Methods. 2021;13:1226–31.
2. Munafo JP Jr, Gianfagna TJ. Chemistry and biological activity of steroidal glycosides from the Lilium genus. Nat prod Rep. 2015;32(3):454–77.
3. Gao J, Zhang T, Jin ZY, Xu XM, Wang JH, Zha XQ, et al. Structural characterisation, physicochemical properties and antioxidant activity of polysaccharide from *Lilium lancifolium* Thunb. Food chem. 2015;169:430–8.
4. Zhou J, An R, Huang X. Genus Lilium: A review on traditional uses, phytochemistry and pharmacology. J Ethnopharmacol. 2021;270:113852.
5. Chen ZG, Zhang DN, Zhu Q, Yang QH, Han YB. Purification, preliminary characterization and in vitro immunomodulatory activity of tiger lily polysaccharide. Carbohydr Polym. 2014;106:217–22.
6. Pan G, Xie Z, Huang S, Tai Y, Cai Q, Jiang W, et al. Immune-enhancing effects of polysaccharides extracted from *Lilium lancifolium* Thunb. Int Immunopharmacol. 2017;52:119–26.
7. Sun X, Gao RL, Xiong YK, Huang QC, Xu M. Antitumor and immunomodulatory effects of a water-soluble polysaccharide from *Lilii Bulbus* in mice. Carbohydr Polym. 2014;102:543–9.
8. Han HP, Xie HC. A study on the extraction and purification process of lily polysaccharide and its anti-tumor effect. Afr J Tradit Complement Altern Med. 2013;10(6):485–9.
9. Li W, Wang Y, Wei H, Zhang Y, Guo Z, Qiu Y, et al. Structural characterization of Lanzhou lily (*Lilium davidii* var. *unicolor*) polysaccharides and determination of their associated antioxidant activity. J Sci Food Agric. 2020;100(15):5603–16.
10. Zhao BT, Zhang J, Guo X, Wang JL. Microwave-assisted extraction, chemical characterization of polysaccharides from *Lilium davidii* var. *unicolor* salisb and its antioxidant activities evaluation. Food Hydrocolloid. 2013;31(2):346–56.
11. Hui H, Li X, Jin H, Yang X, Xin A, Zhao R, et al. Structural characterization, antioxidant and antibacterial activities of two heteropolysaccharides purified from the bulbs of *Lilium davidii* var. *unicolor* Cotton. Int J Biol Macromol. 2019;133:306–15.
12. Wang F, Wang W, Niu X, Huang Y, Zhang J. Isolation and structural characterization of a second polysaccharide from bulbs of Lanzhou lily. Appl Biochem Biotechnol. 2018;186(3):535–46.
13. Zhang T, Gao J, Jin ZY, Xu XM, Chen HQ. Protective effects of polysaccharides from *Lilium lancifolium* on streptozotocin-induced diabetic mice. Int J Biol Macromol. 2014;65:436–40.
14. Shi XD, Yin JY, Cui SW, Wang Q, Wang SY, Nie SP. Plant-derived glucomannans: sources, preparation methods, structural features, and biological properties. Trends Food Sci Tech. 2020;99:101–16.
15. Du XZ, Li J, Chen J, Li B. Effect of degree of deacetylation on physicochemical and gelation properties of konjac glucomannan. Food Res Int. 2012;46(1):270–8.
16. Chokboribal J, Tachaboonyakiat W, Sangvanich P, Ruangpornvisuti V, Jettanacheawchankit S, Thunyakitpisal P. Deacetylation affects the physical properties and bioactivity of acemannan, an extracted polysaccharide from *Aloe vera*. Carbohydr Polym. 2015;133:556–66.
17. Liu C, Cui Y, Pi F, Cheng Y, Guo Y, Qian H. Extraction, purification, structural characteristics, biological activities and pharmacological applications of acemannan, a polysaccharide from *Aloe vera*: a review. Molecules. 2019;24(8):1554.
18. Kumar S, Kumar R. Role of acemannan *O*-acetyl group in murine radioprotection. Carbohydr Polym. 2019;207:460–70.
19. Salah F, Ghoul YE, Mahdhi A, Majdoub H, Jarroux N, Sakli F. Effect of the deacetylation degree on the antibacterial and antibiofilm activity of acemannan from *Aloe vera*. Ind Crops Prod. 2017;103:13–8.
20. Feng L, Yin JY, Nie SP, Wan YQ, Xie MY. Fractionation, physicochemical property and immunological activity of polysaccharides from *Cassia obtusifolia*. Int J Biol Macromol. 2016;91:946–53.
21. Sassaki GL, Gorin PA, Souza LM, Czelusniak PA, Iacomini M. Rapid synthesis of partially O-methylated alditol acetate standards for GC-MS: some relative activities of hydroxyl groups of methyl glycopyranosides on Purdie methylation. Carbohydr Res. 2005;340(4):731–9.
22. Nguyen TA, Thien DT, Dong NT, Dung PL, Nguyen VD. Isolation and characteristics of polysaccharide from *Amorphophallus corrugatus* in Vietnam. Carbohydr Polym. 2011;84(1):64–8.
23. Seedevi P, Moovendhan M, Vairamani S, Shanmugam A. Structural characterization and biomedical properties of sulfated polysaccharide from the gladius of *Sepioteuthis lessoniana* (Lesson, 1831). Int J Biol Macromol. 2016;85:117–25.
24. Shi XD, Nie SP, Yin JY, Que ZQ, Zhang LJ, Huang XJ. Polysaccharide from leaf skin of *Aloe barbadensis* Miller: Part I. Extraction, fractionation, physicochemical properties and structural characterization. Food Hydrocolloid. 2017;73:176–83.

25. Ji X, Guo J, Ding D, Gao J, Hao L, Guo X, et al. Structural characterization and antioxidant activity of a novel high-molecular-weight polysaccharide from *Ziziphus Jujuba* cv. Muzao. J Food Meas Charact. 2022;16(3):2191–200.
26. Mohacek-Grosev V, Bozac R, Puppels GJ. Vibrational spectroscopic characterization of wild growing mushrooms and toadstools. Spectrochim Acta A Mol Biomol Spectrosc. 2001;57(14):2815–29.
27. Ji X, Wang Z, Hao X, Zhu Y, Lin Y, Li G, et al. Structural characterization of a new high molecular weight polysaccharide from *jujube* fruit. Front Nutr. 2022;9:1012348.
28. Hannuksela T, Hervé du Penhoat C. NMR structural determination of dissolved *O*-acetylated galactoglucomannan isolated from *Spruce thermomechanical* pulp. Carbohydr Res. 2004;339(2):301–12.
29. Xing X, Cui SW, Nie S, Phillips GO, Goff HD, Wang Q. Study on dendrobium officinale *O*-acetyl-glucomannan (Dendronan®): part II. Fine structures of *O*-acetylated residues. Carbohydr Polym. 2015;117:422–33.
30. Lundqvist J, Teleman A, Junel L, Zacchi G, Dahlman O, Tjerneld F, et al. Isolation and characterization of galactoglucomannan from spruce (*Picea abies*). Carbohydr Polym. 2002;48(1):29–39.
31. Teleman A, Nordström M, Tenkanen M, Jacobs A, Dahlman O. Isolation and characterization of *O*-acetylated glucomannans from aspen and birch wood. Carbohydr Res. 2003;338(6):525–34.
32. Deng Y, Li M, Chen LX, Chen XQ, Lu JH, Zhao J, et al. Chemical characterization and immunomodulatory activity of acetylated polysaccharides from *Dendrobium devonianum*. Carbohydr Polym. 2018;180:238–45.
33. Shi XD, Yin JY, Zhang LJ, Huang XJ, Nie SP. Studies on *O*-acetyl-glucomannans from amorphophallus species: comparison of fine structure. Food Hydrocolloid. 2019;89:503–11.
34. Ampestrini LH, Silveira JL, Duarte ME, Koop HS, Noseda MD. NMR and rheological study of *Aloe barbadensis* partially acetylated glucomannan. Carbohydr Polym. 2013;94(1):511–9.
35. Shi XD, Yin JY, Zhang LJ, Li OY, Huang XJ, Nie SP. Studies on polysaccharides from leaf skin of *Aloe barbadensis* Miller: part II. Structural characteristics and molecular properties of two lower molecular weight fractions. Food Hydrocolloid. 2019;86:50–61.
36. Kuang MT, Li JY, Yang XB, Yang L, Xu JY, Yan S, et al. Structural characterization and hypoglycemic effect via stimulating glucagon-like peptide-1 secretion of two polysaccharides from *Dendrobium officinale*. Carbohydr Polym. 2020;241:116326.
37. Zhang Y, Zhou T, Wang H, Cui Z, Cheng F, Wang KP. Structural characterization and in vitro antitumor activity of an acidic polysaccharide from *Angelica sinensis* (Oliv.) Diels. Carbohydr Polym. 2016;147:401–8.
38. He PF, He L, Zhang AQ, Wang XL, Qu L, Sun PL. Structure and chain conformation of a neutral polysaccharide from sclerotia of Polyporus umbellatus. Carbohydr Polym. 2017;155:61–7.
39. Cui W, Wood PJ, Blackwell B, Nikiforuk J. Physicochemical properties and structural characterization by two-dimensional NMR spectroscopy of wheat β-D-glucan-comparison with other cereal β-D-glucans. Carbohydr Polym. 2000;41(3):249–58.
40. Li XJ, Bao WR, Leung CH, Ma DL, Zhang G, Lu AP, et al. Chemical structure and immunomodulating activities of an α-Glucan purified from *Lobelia chinensis* Lour. Molecules. 2016;21(6):779.
41. Hui H, Jin H, Li X, Yang X, Cui H, Xin A, et al. Purification, characterization and antioxidant activities of a polysaccharide from the roots of *Lilium davidii* var. *unicolor* Cotton. Int J Biol Macromol. 2019;135:1208–16.
42. Bock K, Pedersen C, Pedersen H. Carbon-13 nuclear magnetic resonance data for oligosaccharides. Adv Carbohyd Chem Bi. 1984;42:193–225.
43. Guo J, Lu L, Li J, Kang S, Li G, Li S, et al. Extraction, structure, pharmacological activity, and structural modification of *Lilium* polysaccharides. Fitoterapia. 2023;172:105760.
44. Tian R, Ding Y, Peng YY, Lu NH. Myeloperoxidase amplified high glucose-induced endothelial dysfunction in vasculature: role of NADPH oxidase and hypochlorous acid. Biochem Biophys Res Commun. 2017;484(3):572–8.
45. Tian R, Ding Y, Peng YY, Lu NH. Inhibition of myeloperoxidase- and neutrophil- mediated hypochlorous acid formation in vitro and endothelial cell injury by (-)-epigallocatechin galate. J Agric Food Chem. 2017;65(15):3198–203.
46. Bush CJ, Binder CJ. 2017 Malondialdehyde epitopes as mediators of sterile inflammation. Biochim Biophys Acta Mol Cell Biol Lipids. 1862;4:398–406.
47. Islamiana D, Prabowo R, Pramaningtyas MD. The effect of orange water kefir on malondialdehyde (MDA) level and superoxide dismutase (SOD) inhibition rate in kidney tissue of the hyperlipidemic rat (Rattus norvegicus). Atherosclerosis. 2020;315:e264.
48. Gao Y, Liu Y, Ma F, Sun M, Song Y, Xu D, et al. Lactobacillus plantarum Y44 alleviates oxidative stress by regulating gut microbiota and colonic barrier function in Balb/C mice with subcutaneous d-galactose injection. Food Func. 2021;12:373–86.
49. Jaikua W, Kueakhai P, Chaithirayanon K, Tanomrat R, Wongwairot S, Riengrojpitak S, et al. Cytosolic superoxide dismutase can provide protection against *Fasciola gigantica*. Acta Trop. 2016;162:75–82.
50. Fernando IPS, Jayawardena TU, Wu JP. Marine proteins and peptides: production, biological activities, and potential applications. Food Innov Adv. 2023;2(2):69–84.
51. Ji XL, Guo JH, Cao TZ, Zhang TT, Liu Y, Yan YZ. Review on mechanisms and structure-activity relationship of hypoglycemic effects of polysaccharides from natural resources. Food Sci Hum Well. 2023;12(6):1969–80.
52. Cuciniello R, Di Meo F, Filosa S, Crispi S, Bergamo P. The antioxidant effect of dietary bioactives arises from the interplay between the physiology of the host and the gut microbiota: involvement of short-chain fatty acids. Antioxidants (Basel). 2023;12:1073.
53. Li JL, Wang JJ, Zhang N, Li Y, Cai ZZ, Li GH, et al. Anti-aging activity and their mechanisms of natural food-derived peptides: current advancements. Food Innov Adv. 2023;2(4):272–90.
54. An L, Zhou M, Marikar FMMT, Hu XW, Miao QY, Li P, et al. Salvia miltiorrhiza lipophilic fraction attenuates oxidative stress in diabetic nephropathy through activation of nuclear factor erythroid 2-related factor 2. Am J Chin Med. 2017;45(7):1441–57.
55. Han D, Chen W, Gu X, Shan R, Zou J, Liu G, et al. Cytoprotective effect of chlorogenic acid against hydrogen peroxide-induced oxidative stress in MC3T3-E1 cells through PI3K/Akt-mediated Nrf2/HO-1 signaling pathway. Oncotarget. 2017;8(9):14680–92.
56. Chung HT, Pae HO, Cha YN. Role of heme oxygenase-1 in vascular disease. Curr Pharm Des. 2008;14(5):422–8.
57. Hseu YC, Chou CW, Senthil Kumar KJ, Fu KT, Wang HM, Hsu LS, et al. Ellagic acid protects human keratinocyte (HaCaT) cells against UVA-induced oxidative stress and apoptosis through the upregulation of the HO-1 and Nrf-2 antioxidant genes. Food Chem Toxicol. 2012;50(5):1245–55.


## Publisher's Note